Int. J. Multiphase Flow Vol. 8, No. 2, pp. 147–163, 1982
Printed in Great Britain.

0301-9322/82/020147-17$03.00/0
Pergamon/Elsevier

HYDRODYNAMICS OF A BUBBLE FORMED AT VENT PIPE EXIT†

CHIA-LIN CHEN and VIJAY K. DHIR

Chemical, Nuclear and Thermal Engineering Department, University of California, Los Angeles, CA 90024, U.S.A.

(*Received* 1 *July* 1980; *in revised form* 15 *June* 1981)

Abstract—In this paper, the hydrodynamics of a bubble formed during transient injection of air through a tube submerged in a pool of water has been studied. The experiments were performed by injecting air through vertical tubes varying in diameter from 0.9 to 9.5 cm and located in the middle of a 45 cm dia. and 120 cm high plexiglas chamber. The plexiglas chamber was partly filled with water and was open at the top to the outside. Data for bubble growth and vent line pressure histories are obtained under different upstream pressure conditions. Effect of presence of an orifice in the vent line on bubble growth has also been investigated.

A theoretical model describing the bubble growth at the exit of a vent pipe submerged in a pool of water is developed. Predictions of bubble radius, line static pressure and uplift on the bottom of the test chamber have been made and are found to compare well with the data. Insertion of an orifice in the pipe line between the solenoid valve and the vent exit has been found to inhibit the bubble expansion as well as alter the bubble oscillation characteristics.

1. INTRODUCTION

Current boiling water reactor (BWR) containment designs utilize a water pool for pressure suppression in the event of a loss of coolant accident (LOCA). In the event of a LOCA, the steam from the primary coolant pressurizes the dry well. This increased pressure pushes the water initially filling the vent pipe into the suppression pool. The vent clearing is followed by injection of air or air-steam mixture into the pool. Air which is initially in the vent and is at higher pressure, expands and rises up in the pool in the form of a bubble. The water slug ejection due to air pressure produces a downward load on the torus, while the expansion of air in the form of a bubble at vent exit displaces the pool free surface upward. The accelerating free surface could cause an impact load in the structure, e.g. on the internal ring header and the support columns. Also, the upward acceleration of liquid can cause an uplift on the torus. The uplift of the BWR Mark I torus may pose serious safety questions. Thus, the analysis of the dynamics of an air bubble formed at the exit of a vent pipe is important to understand the impact load on the ring header and uplift on the torus.

Many studies dealing with various aspects of air bubble formation and growth under water have been published in the past. Some of those studies were motivated by concern for the behavior of the spherical explosions in a uniform unlimited medium. Whereas others have been confined to the bubble formation at an orifice under the influence of viscosity, surface tension, and the liquid density. Several studies have also been made on dynamics of a bubble nucleating in a superheated liquid.

As early as 1917 Rayleigh derived an important non-linear ordinary differential equation which governed the phenomena of spherical bubble expansion in a uniform infinite medium. Almost all other workers started their research based on this fundamental equation. Lamb (1945) coupled the Rayleigh equation with isentropic thermodynamic relations between the pressure and the volume of an ideal gas. For an irrotational flow around a spherical bubble, the Rayleigh equation governing the growth or collapse of the bubble is obtained from continuity and momentum equations of liquid as

$$\frac{\rho_L}{R}\frac{\mathrm{d}}{\mathrm{d}t}\left(R^2\frac{\mathrm{d}R}{\mathrm{d}t}\right)-\frac{1}{2}\rho_L\left(\frac{\mathrm{d}R}{\mathrm{d}t}\right)^2-(P_R-P_\infty)=0. \qquad [1]$$

†This work was supported by Water Reactor Safety Research Division of USNRC.

In [1], ρ_L is the density of the liquid, R is the radius of the bubble, P_R is the liquid side pressure on the bubble surface, P_∞ is the ambient pressure and t is the time.

Effect of liquid viscosity can be introduced into [1] through the boundary condition at the liquid–gas interface. Gilmore (1952) was the first to incorporate the effect of liquid viscosity, μ_L, and interfacial tension, σ, in the relation between liquid side pressure, P_R, and bubble side pressure P_b,

$$P_R = P_b - \frac{2\sigma}{R} + 4\mu_L \frac{\dot{R}}{R} \qquad [2]$$

Substitution of [2] into [1] yielded the modified Rayleigh equation

$$R\ddot{R} + \frac{3}{2}\dot{R}^2 + \frac{4\mu_L}{\rho_L}\frac{\dot{R}}{R} + \frac{2\sigma}{\rho_L R} = \frac{P_b - P_\infty}{\rho_L}. \qquad [3]$$

Equation [3] was also subsequently derived by Scriven (1959). The above derivation of [3] is based on the assumption that pressure inside the bubble is uniform. Plesset & Zwick (1954) have pointed out that this is a reasonable assumption when the gas density is very small such that effect of its inertia may be negligible. Furthermore, if the velocity of the bubble surface is much less than the sonic velocity of the gas, any pressure variations would be immediately felt at all points within the bubble before an appreciable movement of the interface has taken place.

Plesset & Zwick (1954) as well as Forster & Zuber (1954) have studied the vapor bubble growth in superheated liquid. They used [3] with the assumption that viscosity of the liquid could be neglected and showed that in the asymptotic limit bubble growth was controlled solely by diffusion of heat through the superheated liquid. Both these studies concluded that for large times the radius of a bubble growing in a superheated liquid will increase as square root of time. This was later confirmed by Birkhoff *et al.* (1958), who obtained a similarity solution for the complete problem in which effect of convection was also included.

The modified Rayleigh equation [3] obtained above is based on the assumption that the center of the bubble remains fixed with time. However, there are many situations when the position of the bubble mass center may change. Herring (1941) was the first one to include gravity force in an expanding underwater explosion. Later McCann & Prince (1969) used the potential flow theory to describe the formation of a bubble at a submerged orifice. Neglecting viscous force and the wall effect of the orifice plate, they obtained expression for liquid side bubble pressure in terms of the distance, S, of the bubble center from the orifice as:

For $S < R$

$$P_R = P_b - \frac{2\sigma}{R} + \rho_L g S + \frac{\rho_L U^2 R}{4(S+R)}\left(1 + \frac{1}{2}\frac{S}{R} - \frac{3}{2}\frac{S^3}{R^3}\right). \qquad [4]$$

For $S > R$

$$P_R = P_b - \frac{2\sigma}{R} + \rho_L g S + \frac{\rho_L U^2}{4}. \qquad [5]$$

In [4] and [5], U is the velocity of the center of the bubble mass. Substitution of [4] or [5] into [1] yields growth equations for bubbles smaller than or greater than a hemisphere and moving with a velocity U in an infinite liquid.

Experimental investigations of bubble formation at a submerged orifice have been made by Davidson & Schuler (1960). In their work bubble formation under constant pressure and constant flow rate was studied for the limiting cases of low and high flow rates. The effect of

viscosity, surface tension, orifice size and liquid density on bubble diameter at departure was also determined. Further experimental work and modeling of bubbles formed at submerged orifices was done by Ramakrishna *et al.* (1969) and by Satyanaryana *et al.* (1969). From these later studies it was concluded that surface tension is only important for small gas flow rates and that surface tension tends to increase the bubble size at departure. The effect of liquid viscosity is small at low flow rates but at high flow rates its effect is to increase the bubble size. For low viscosity liquids and for small diameter orifices, liquid density was found to have no influence on bubble volume at high flow rates. For highly viscous liquids, when orifices of small diameter were used, an increase in liquid density was found to result in decrease in bubble volume at departure.

Bubble growth at the end of a vent pipe submerged in liquid and connected to a gas reservoir was first studied by Weisshanpl (1972). In his work Weisshanpl assumed that mass flow rate into the bubble would always compensate for the reduction in bubble pressure due to expansion of the bubble. In other words, this implied that during the growth process the pressure within the bubble remained constant. This assumption may not be true in general, as the pressure inside the gas bubble will change with time when the supplied flow rate cannot keep up with the expansion of the bubble. Recent interest in the modeling of hydrodynamic forces experienced by a BWR pressure suppression pool torus during transient injections of air or steam has resulted in several studies of bubble growth at vent pipe exit. However, most of these studies attempt ot model complete sequence of events: drywell pressurization, vent clearing, forces at the bottom of the wet well and wet well pressurization and treat bubble growth only implicitly or under system specific assumptions. In the study of Kiang & Grossi (1978) air bubble volume at a given time was calculated by *a priori* using the measured wet well pressure history and an adiabatic compression model for the wet well air space. The conservation equations of mass and energy were integrated numerically. However, the authors did not report the results for bubble volume or bubble pressure as a function of time. Sargis *et al.* (1978) have developed a thermal-hydraulic model to describe steam chugging phenomena. They solved conservation of mass and energy equations for steam volume in the vent pipe and in the pool. The steam bubble in the pool was assumed to be hemispherical. The assumption of a hemispherical bubble may not be appropriate when condensation does not take place at the interface as in the case of pure air injection. Data on growth of an air bubble at vent pipe exit have been obtained by Chan *et al.* (1977), but they do not propose any model for bubble growth.

The objective of the present work is to study both experimentally and theoretically the dynamics of an air bubble growing at an exit of a vent pipe. Effect of presence of an orifice in the vent line will also be investigated. Use of orifices in vent pipes has been suggested by Anderson *et al.* (1977) to avoid some of the practical difficulties associated with scaling of temperatures in the prototype suppression pool with those in the models.

2. ANALYTICAL MODEL

A model is developed to analyze the phenomena of vent clearing and bubble growth during transient injection of air into a pool of water. First, a description of the idealized process is given. The model and the governing equations for each stage of air injection are discussed in detail, and numerical approach used to solve them is outlined. Finally, uplift force due to a bubble expanding in a finite volume of liquid is modeled.

2.1 *Description of the process*

Figure 1 shows the geometrical configuration used to simulate the process of transient injection of air into a pool of water. An orifice between the air reservoir and the pipe line connecting the air reservoir to a pool of water is used to model a quick-opening or closing solenoid valve. Generally, the flow area of solenoid valve in full open position may be less than the area of the connecting pipe line. Also the solenoid valve may take several milliseconds to open fully after it is energized. The air injection process starts when the solenoid valve is

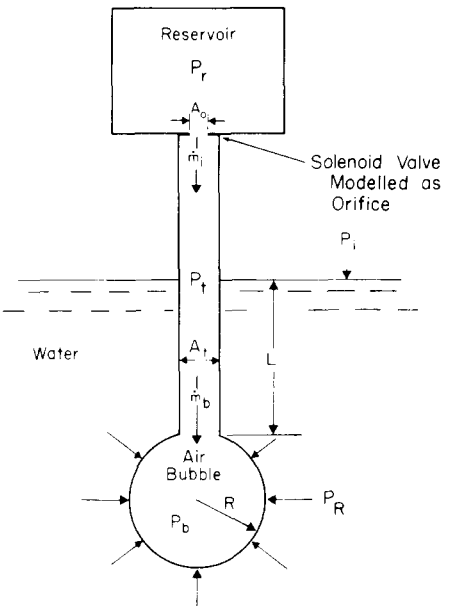

Figure 1. Model for a bubble growth at vent pipe exit.

activated. In this study the solenoid valve diameter is assumed to increase linearly with time from zero to a maximum value. As soon as the solenoid valve starts to open, the pressure inside the pipe line begins to increase. A pressure disturbance initiated at the orifice moves inside the pipe with sonic speed until it reaches the surface of the water. When the pressure signal reaches the upper surface of the water slug, the vent clearing stage begins. During the vent clearing, pressure inside the pipe continues to increase. After complete vent clearing, bubble starts to grow at vent pipe exit. The bubble would leave the vent when buoyancy exceeds the pressure and inertia forces acting on the bubble.

In the present work, the flow of air into the reservoir was cut-off when pressure in the reservoir reached a desired value. Thus during the vent clearing and bubble growth stages pressure inside the reservoir can be safely assumed to remain constant. This may not be true for the drywell in a prototype where pressure in the drywell continues to increase with time.

2.2 *Model for vent clearing*

The vent clearing model employed in this work is similar to the model developed earlier by Chan *et al.* (1977). Any instability of the interface as may occur during vent clearing is ignored. Figure 2 shows the physical model for vent clearing. Water slug in the vent clearing stage is assumed to behave as a rigid body. Friction at the pipe wall is neglected. The time dependent momentum equation for the water slug represented by control volume *abcd* as shown in figure 2 can be written as

$$\frac{\mathrm{d}}{\mathrm{d}t}(m_t u) + \rho_L u^2 A_t = [P_t(t) - (P_i + \rho_L g X)]A_t \qquad [6]$$

where m_t is the total mass of the liquid being moved with a velocity, u, A_t is the cross-sectional area of the vent pipe, P_t is the pressure in the vent pipe, P_i is the pressure above the free surface of water in the pool, g is the gravitational acceleration and X is the distance measured from the original position of the free surface of the water slug. The total mass, m_t, is composed of two parts: the real mass, m_r, of the water slug during transient and the virtual mass, m_v. For a

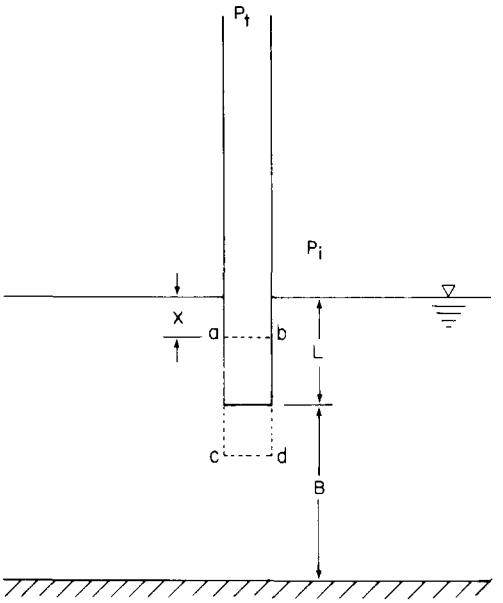

Figure 2. Model for vent clearing.

submergence depth, L, the real mass is given by

$$m_r = \rho_L(1 - X)A_t \qquad [7]$$

while an expression for the virtual mass is written as

$$m_v = \beta\rho_L A_t X. \qquad [8]$$

In [8] β is a constant which generally varies between zero and one (see Dhir *et al.* 1977). Substituting [7] and [8] into [6] and writing $u = \mathrm{d}X/\mathrm{d}t$, [6] can be rewritten as

$$[L + (\beta - 1)X]\ddot{X} + \beta\dot{X}^2 + gX = \frac{P_t(t) - P_i}{\rho_L}. \qquad [9]$$

If β is taken to be unity so as to have a conservative estimate of the vent clearing time, [9] reduces to

$$L\ddot{X} + \dot{X}^2 + gX = \frac{P_t(t) - P_i}{\rho_L} \qquad [10]$$

where L is the submergence depth of the vent pipe. Equation [10] can be solved once $P_t(t)$ is known as a function of time.

Pressure inside the pipe line is obtained by making a mass balance on the control volume, which coincides with the volume occupied by air within the pipe. The mass conservation equation for the pipe volume between the orifice and water slug is

$$\frac{\mathrm{d}}{\mathrm{d}t}\left[\frac{P_t(t)V_t(t)}{R_G T_t}\right] = \dot{m}_b(t) - \dot{m}_i(t) \qquad [11]$$

where $V_t(t)$ is the vent volume between the orifice and the free surface of the water slug, R_G is the gas constant for air, T_t is the stagnation temperature of air in the vent pipe, $\dot{m}_b$ is the mass flow rate of air into the bubble and $\dot{m}_i$ is the mass flow rate of air through the orifice and into the vent pipe. During the time the interface does not move, $V_t(t)$ is constant. When water slug

starts to move, $V_t(t)$ depends on the length of the pipe emptied. The value of $\dot{m}_b(t)$ is equal to zero until vent is cleared. After the water slug has been ejected completely, the volume of the pipe line, $V_t(t)$, remains constant while $\dot{m}_b(t)$ now is a function of time and depends on the growth characteristics of the bubble. Assuming that (1) air flow through the orifice is isentropic; (2) friction is negligible; (3) the process is adiabatic; and (4) stagnation temperature in the pipeline is room temperature and remains constant. The mass flow rate through the solenoid valve (modeled as an orifice) can be written as

$$\dot{m}_i(t) = C_0 A_0 \sqrt{(\gamma/R_G)} \frac{P_r}{\sqrt{(T_r)}} \frac{M_0}{\left(1+\frac{\gamma-1}{2} M_0^2\right)^{(\gamma+1)/2(\gamma-1)}}. \quad [12]$$

In [12] C_0 is the discharge coefficient of the orifice, A_0 is the cross-sectional area of the orifice, γ is the coefficient of isentropic expansion of air, P_r is the pressure in the reservoir upstream of the orifice, T_r is the temperature of the reservoir and M_0 is the Mach number of the flow through the orifice. Equation [12] is written in terms of the Mach number of the orifice as it facilitates evaluation of the mass flow rate under both nonchoked and choked conditions. For air, choking of the solenoid valve will occur when ratio of pressures upstream and downstream of the solenoid valve exceeds 1.89. The functional form of [12] can easily be obtained by following Shapiro (1953). In [12], coefficient of discharge of the solenoid valve (modeled as an orifice) is a function of both the reservoir pressure and the stagnation pressure in the pipe. The stagnation pressures in the pipe and the reservoir are related through the Mach number, M_0, at the orifice as

$$\frac{P_r}{P_t} = \left[\frac{1+\frac{\gamma-1}{2} M_0^2}{1+\frac{\gamma-1}{2} C_0^2 M_0^2} \right]^{\gamma/(\gamma-1)}. \quad [13]$$

The gas flow rate out of the pipe and into the bubble can be found in terms of the pressure in the pipe. From an equation similar to [12], $\dot{m}_b(t)$ is obtained as

$$\dot{m}_b(t) = C_t A_t \sqrt{(\gamma/R_G)} \frac{P_t}{\sqrt{(T_t)}} \frac{M_t}{\left(1+\frac{\gamma-1}{2} M_t^2\right)^{(\gamma+1)/2(\gamma-1)}} \quad [14]$$

The pressure in the pipe and the bubble are related through the Mach number, M_t, at the pipe exit as

$$\frac{P_t}{P_b} = \left[\frac{1+\frac{\gamma-2}{2} M_t^2}{1+\frac{\gamma-1}{2} C_t^2 M_t^2} \right]^{\gamma/(\gamma-1)}. \quad [15]$$

In [14] and [15], C_t is the pressure loss coefficient which depends on the pipe diameter, the pressure difference between the pipe and the bubble and the size of the bubble. The stagnation temperature, T_t, of air in the pipe and the reservoir temperature, T_r, are assumed to be equal to the ambient temperature and are assumed to remain constant with time.

2.3 *Model for bubble growth*

When the water slug is ejected completely, the air bubble begins to form at the exit of the vent pipe. The growth rate of the bubble is determined by the surface tension, the liquid inertia, the mass flow rate, and the driving pressure. However, following assumptions are made to simplify the analysis for bubble growth.

(1) The surface tension of water is so small that the pressure drop, $2\sigma/R$, across the bubble wall is negligible.

(2) The bubble is assumed to grow as a sphere. Visual observations show that air bubble starts as a disc before acquiring a strawberry shape. However, the bubble diameter to height ratios plotted by Chen (1979), show that in the later stages of growth the bubble is nearly spherical. In the model the spherical bubble is considered to possess the same value as the actual bubble.

(3) The pressure inside the bubble is uniform.

(4) The temperature, density, and pressure within the bubble are related through isentropic relations and the ideal gas law.

(5) Liquid and gas viscosities are negligible.

(6) The distance between the bubble center and the exit of the vent pipe is equal to the bubble radius.

(7) The center of the air bubble moves with velocity $\dot{R}$.

The last two assumptions are not strictly true when bubble just starts to form at the vent pipe exit but should be quite realistic during the later stages of growth.

Employing the above assumptions and combining [4] or [5] for $S = R$ with [1], the equation describing bubble growth can be written as

$$P_b(t) = \rho_L\left(\frac{5}{4}\dot{R}(t)^2 + R(t)\ddot{R}(t) + g(L+R)\right) + P_i. \qquad [16]$$

The pressure inside the bubble can be obtained by combining the gas law and the mass conservation equation for the bubble as

$$\frac{\mathrm{d}}{\mathrm{d}t}\left[\frac{P_b(t)V_b(t)}{R_G T_b(t)}\right] = \dot{m}_b(t). \qquad [17]$$

In the above equation, T_b denotes the air temperature in the bubble. The bubble volume, V_b, is related to the bubble radius as

$$V_b = \frac{4}{3}\pi R^3. \qquad [18]$$

The bubble temperature can be determined by making an energy balance for the bubble. Assuming that initially the temperature of the bubble is the ambient temperature and the bubble expands adiabatically, the rate of change of temperature of the bubble with reference to the reservoir, the vent pipe or the pool temperature can be written as

$$\frac{\mathrm{d}T_b}{\mathrm{d}t} = -\frac{(P_b - P_i - (L+R)\rho_L g)4\pi R^2 \dot{R}}{\int_0^t C_v \dot{m}_b(t)\,\mathrm{d}t} \qquad [19]$$

where C_v is the specific heat of air at constant volume.

2.4 *Solution approach*

With temperature, T_t, in the pipe equal to the temperature, T_r, of the reservoir and the initial vent volume, V_{ti}, between the solenoid valve and the water slug being known, [10]–[19] represent ten relations in ten unknowns (X, P_t, $\dot{m}_i$, $\dot{m}_b$, M_0, M_t, P_b, V_b, R, T_b). These equations can be solved numerically, if the reservoir pressure, ambient temperature and initial pressure in the vent line are known at the time of activation of the solenoid valve. Prior to complete vent clearing, $\dot{m}_b$, is zero and only [10]–[13] are solved. Equation [10] is integrated by a fourth-order

Runge–Kutta method with initial conditions $X = 0$ and $\dot{X} = 0$. It must be mentioned that during vent clearing, the vent volume, V_t, can be written as a sum of initial vent volume, V_{ti}, and the volume of the vent emptied by the water slug.

$$V_t = V_{ti} + A_t X. \tag{20}$$

After vent clearing, the vent volume remains constant

$$V_t = V_{ti} + A_t L$$

and [10] need not be solved.

During the bubble growth period [11]–[19] are solved simultaneously. Equation [16] which governs the bubble growth is again integrated by a fourth-order Runge–Kutta method. However, [16] has a singularity at the beginning, as it cannot be solved from the point where the bubble radius is zero. Also, a spherical bubble with a radius less than the tube radius cannot be defined. To overcome these difficulties the following methodology is used. For a very short time period (≈3 ms) after the ejection of water slug, the mass flow rate at the exit of the vent pipe is assumed to remain constant. For this short period, mass conservation equation for the bubble is written as

$$\rho_G \frac{4}{3} \pi R^3 = \rho_G A_t u_c t$$

or

$$R = \left(\frac{3}{4\pi} A_t u_c t\right)^{1/3} \tag{21}$$

where u_c is the terminal ejection velocity of the water slug. Equation [21] connecting the vent clearing stage with the bubble growth stage is used to calculate the bubble radius until bubble radius is greater than the tube radius or the bubble growth rate given by [21] matches with that given by [16] when pressure inside the bubble is assumed to be equal to that in the vent pipe and the term $R\ddot{R}$ is assumed to be much less than $5/4\dot{R}^2$. Thereafter [16] is integrated in steps while using the initial conditions for R and $\dot{R}$ given by [21].

2.1 *Uplift due to expansion of the bubble*

As the air bubble starts to grow with time, water around the bubble will be pushed away. Since water can only move upwards, the result of the water motion will be an uplift on the test chamber. This upward force on the test chamber can be calculated by knowing the inertia of the liquid moving in the upward direction. Exact fluid motion in the presence of constraining walls is difficult to ascertain unless the equations of motion of the liquid are solved with proper boundary conditions. However, an approximate estimate of the upwards force can be made for the geometry considered in this work by knowing that all the liquid displaced to make place for the growing bubble has to move upwards. Assuming that no dissipation of momentum occurs in the liquid, the rate of change of momentum of the liquid moving upwards can be equated to the rate of change of momentum of the virtual mass of the liquid surrounding the bubble. Taking the virtual mass to be the mass of the liquid having a volume equal to the bubble, the upward force, F, due to expansion of the bubble can be written as

$$F = \rho_L \frac{\mathrm{d}}{\mathrm{d}t}\left(\frac{4}{3} \pi R^3 \dot{R}\right). \tag{22}$$

The average upward pressure experienced by the bottom of the test chamber can simply be obtained by dividing the force, F, by the area of the bottom of the test chamber.

3. EXPERIMENTAL APPARATUS AND PROCEDURE

The experimental apparatus was designed so that the vent clearing, the bubble formation, and other associated phenomena could be studied from a single vertical vent submerged in an axisymmetric pool. The apparatus consists of a transparent cylindrical test chamber and a gas supply system. The gas supply system is composed of a 51 mm nominal diameter galvanized iron pipe and a reservoir with a safe working pressure of 200 kPa.

3.1 *Description of the apparatus*

A schematic diagram of the experimental apparatus is shown in figure 3. The test chamber is made of a plexiglas pipe, 45 cm in diameter and 120 cm in height. The plexiglas pipe is held at the ends by two airtight flanges made out of 2.5 cm thick aluminum plate. Five holes are tapped in each of the two flanges for insertion of the pressure transducers. A 51 mm dia. tube holder is welded to the top flange through which vent pipes can be inserted into the test chamber. Ten 19 mm dia. holes are also tapped in the top flange. These holes are generally open to the atmosphere, but can be closed when experiments are to be conducted at pressures other than one atmosphere. The tube holder on the upper flange is connected to the 51 mm dia. air supply line via a Thermo Systems Model 1051-1 Anemometer. The maximum response frequency of the anemometer in air is 10 kHz, and the anemometer is capable of measuring a maximum velocity of 300 m/s. A Statham pressure transducer is placed downstream of the anemometer to measure the line static pressure, while three similar pressure transducers are placed on the bottom plate and one pressure transducer is placed on the top plate. The Statham differential pressure transducers are fully active strain-gauge type transducers. A 5 V DC excitation is required for these transducers. The response time of these pressure transducers is estimated to be 0.6 ms based on the information from the vendor. The analog output of the pressure from pressure transducers and the output of the flow velocity from the anemometer are monitored on a Tektronix 564 storage oscilloscope. The time response of this oscilloscope is 0.5 ms.

The air reservoir is a cylindrical steel tank, 0.3 m^3 in volume. The safe working pressure for the reservoir is 200 kPa, and the pressure is controlled by the actuation of a safety relief valve attached to the vessel. The reservoir can be pressurized by the opening of a solenoid valve, connected to the utility air supply system of the laboratory. A 31.75 mm dia. quick-acting solenoid valve connects the reservoir to the test chamber through the 51 mm nominal diameter pipe line. The solenoid valve opens completely within 32–60 ms after it is activated. A provision is made to place an orifice plate in the pipe line between the solenoid valve and the exit of the vent pipe. Orifices of 2.54 and 1.56 cm dia. were used in the experiments.

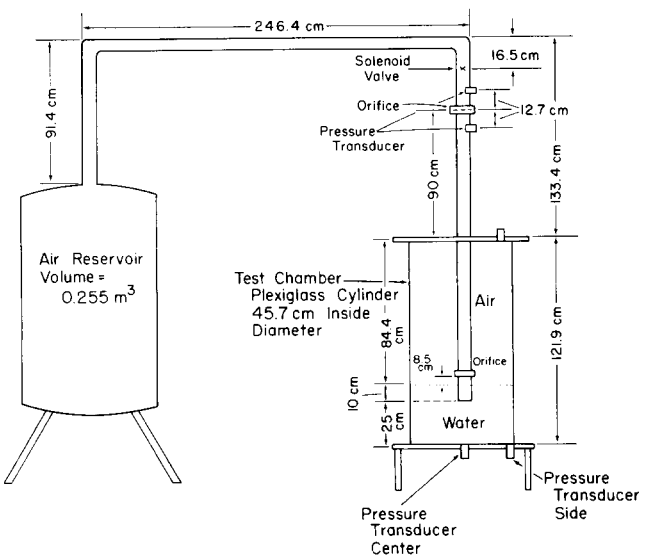

Figure 3. Schematic diagram of the apparatus.

A 16 mm HYCAM high speed motion picture camera was used to record the processes of the vent clearing, the bubble formation, and the free surface movement. The film speed could be adjusted by a frame rate controller from 30 to 3000 frames/sec. A timing light generator was also used to obtain the actual frame speed. Additional details of the experimental setup are given by Chen (1979).

3.2 *Experimental procedure*

Before conducting the experiment, the flowmeter, pressure transducers, oscilloscope, and movie camera were synchronized, and their operability checked. A plexiglas tube of the desired size, with a centimeter scale posted on it, was inserted through the tube holder on the upper flange and was held rigidly. The tube length was adjusted to place the exit plane of the tube at a desired distance from the bottom of the test chamber. The test chamber was then filled with fresh water to give a pre-selected submergence depth to the tube. Then, the air reservoir was pressurized. The movie camera and all other systems, together with the quick-acting solenoid valve were activated. The vent-clearing and bubble growth processes were captured on a fast movie film at a maximum speed of 1500 frames/sec, while the exposure time was kept at about 1/3750 sec. The flow rate and pressure traces were recorded on the oscilloscope screen. A polaroid picture of the traces on the oscilloscope screen was taken for data reduction and for permanent record of the data.

3.3 *Data reduction*

Photographic information was used to determine the bubble growth rate. The procedure consisted of projecting movies on a screen and starting from a frame in which the bubble began growing, the image of the bubble was plotted on a graph paper held on the screen. The horizontal, as well as the vertical bubble diameters, were measured. Then assuming an axisymmetric bubble, the bubble volume was calculated by rotating the drawing with respect to the center line of the vent pipe. From the bubble volume, the average radius of an equivalent sphere was calculated. The number of frames between two consecutive sizes were counted. The exact frame speed was determined from the neon timing-light marks on the film. The pressure and flow rate histories were reduced from the polaroid picture of the traces obtained on the oscilloscope screen. The maximum error in all of the data on pressures and bubble radii is calculated by Chen (1979) to be less than ± 10 per cent.

4. RESULTS AND DISCUSSION

Fourteen different experiments were conducted with reservoir pressures varying between 115.1 and 177.2 kPa and the initial test chamber pressure varying from 87.8 to 101.4 kPa. The inner diameter of the vent pipes was varied from 9 to 95 mm. A few experiments were performed when 2.54 or 1.56 cm dia. orifice plates were placed in the pipe line. In all cases the submergence depth was kept to be 10 cm and the distance of the exit of the vent pipe from the bottom of the test chamber was kept at 25 cm. All of the experiments were conducted by injecting air into water held at a room temperature of about 25°C. Numerical computations of the line static pressure and bubble radius were made for several of the experimental conditions and are compared with the data.

4.1 *Bubble growth and pressure histories*

Visual observation of bubble shape during different stages of growth are shown in figure 4. The individual movie frames shown in figure 4 are for the case when air was injected through a 46 mm vent with a reservoir pressure of 122.0 kPa. The test chamber pressure in this case was 101.4 kPa. It is noted that the bubble starts as a disc and finally acquires a strawberry shape. The ratio of bubble diameter to bubble height for various reservoir and test chamber pressure and for different tubes has been found to remain close to unity during most of the later stages

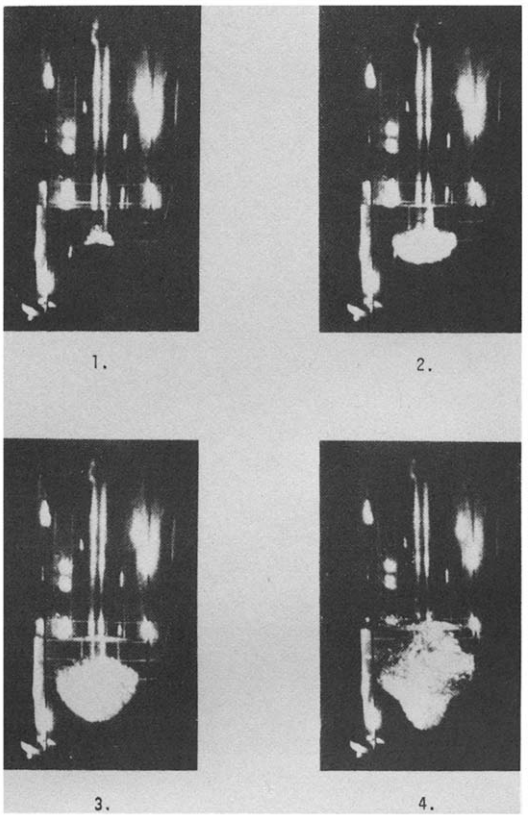

Vent Pipe Diameter = 4.6 cm
Resevoir Pressure = 177.2 kPa
Test Chamber Pressure = 101.4 kPa
Figure 4. History of bubble formation at vent pipe exit.

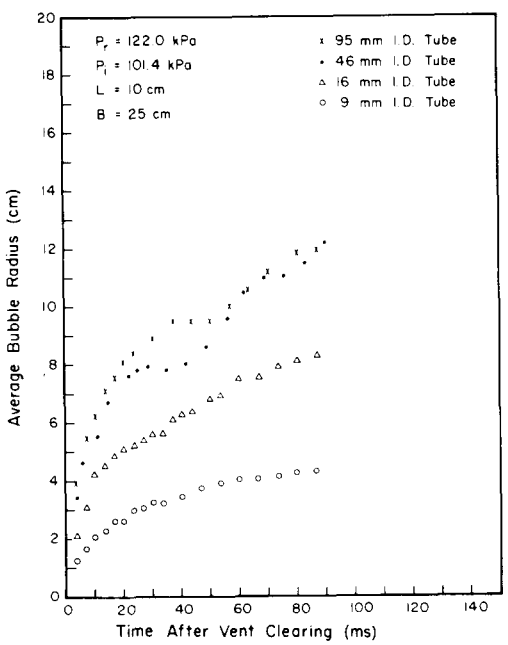

Figure 5. History of average bubble radius for tubes of different diameters.

of growth. After vent clearing, the average bubble diameter $(6V_b/\pi)^{1/3}$ as a function of time is plotted in figure 5 for tubes 9, 16, 46 and 95 mm in diameter. It is observed that bubble growth is oscillatory in nature, however, the magnitude of the oscillation diminishes with decrease in tube diameter.

Figures 6 and 7 compare the predictions of bubble radius and the vent line static pressure

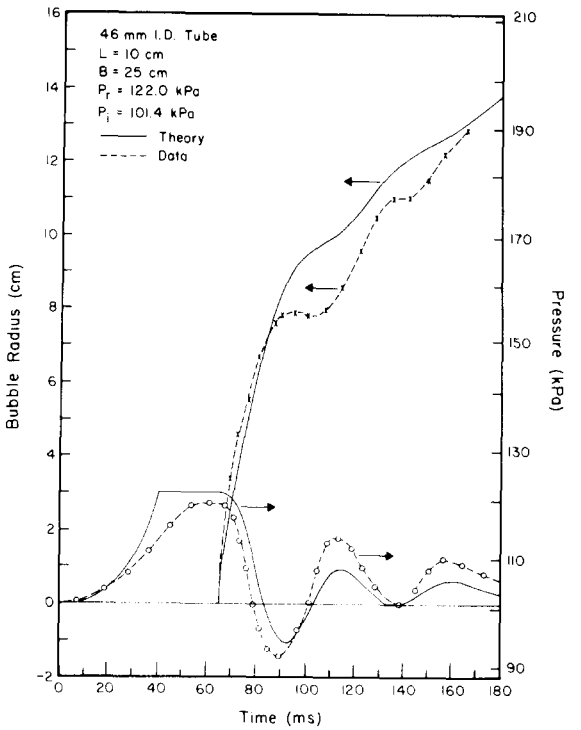

Figure 6. Comparison of theory with observed bubble radius and static pressure histories for a 46 mm i.d. tube.

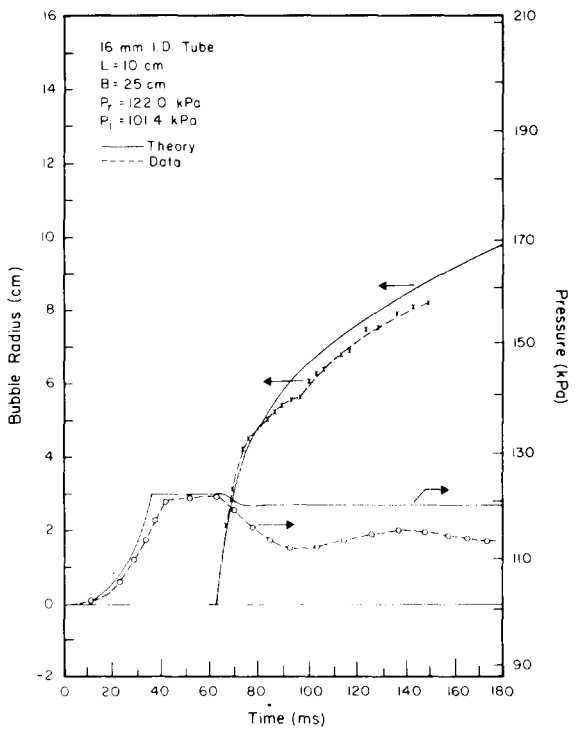

Figure 7. Comparison of theory with observed bubble radius and the static pressure histories for a 16 mm i.d. tube.

with the data obtained with vent tubes of 46 and 16 mm ID, respectively. The predictions are obtained by numerically solving [10]–[19] and by assuming that the solenoid valve takes 60 ms to open completely. During this period the opening of the solenoid valve is assumed to increase linearly to its final diameter of 3.12 cm. The discharge coefficient of the orifice used to simulate valve is a function of the ratio of the pressure upstream and downstream of the solenoid valve.

The functional dependence of the coefficient of discharge was taken from Shapiro (1953). The discharge coefficient, C_t, at the exit of the pipe to account for the pressure loss due to sudden expansion was assumed to be equal to 0.8 for all the cases studied. Furthermore, the stagnation temperatures in the reservoir and in the vent pipe were taken to be 298 K. The data plotted in these figures are for a reservoir pressure of 122 kPa while the pressure of the free space above the pool was 101.4 kPa, the submergence depth was 10 cm and the distance of the vent exit from the bottom of the test chamber was 25 cm. The zero time in figures 6 and 7 corresponds to the times at which the solenoid valve was signalled to open.

As the solenoid valve starts to open, the flow of air causes the pressure in the region between the liquid slug and the solenoid valve to increase. Pressure difference between the vent space above the water slug and the ambient causes the water slug to move into the pool. During the vent clearing process the pressure in the vent pipe continues to increase until it reaches nearly the pressure in the air reservoir. The history of the predicted pressure in the vent pipe during early clearing stage is somewhat different than pressure history observed experimentally. This is probably due to the opening characteristics of the solenoid valve being different than modeled in the analysis. The difference in early pressure histories is of no particular significance since valve opens fully before complete vent clearing occurs. The vent clearing times predicted from this analysis compare well with the data of Chan *et al.* (1977), and Dhir *et al.* (1979).

With 46 mm dia. tube, the bubble radius as well as line static pressure show significant oscillations. However, these oscillations tend to die out with time. The predicted frequency of oscillations matches very favorably with the data. During a bubble expansion period, pressure in the vent line drops below the ambient test chamber when flow rate through the solenoid valve cannot keep up with the flow rate needed to sustain a given growth rate. Bubble pressure lower than surrounding fluid causes a slowdown in bubble growth, which eventually leads to slight shrinking of the bubble. Reduced flow rate into the bubble helps the pressure in the vent line to recover. The line pressure drops again as bubble starts to expand further.

A local minimum in bubble radius generally occurs a little later than a minimum in the line static pressure. This is due to the fact that line pressure starts to recover before bubble growth stops completely. Comparison of figures 6 and 7 shows that bubble volumes 180 ms after activation of the solenoid valve are not proportional to the cross-sectional area of the vent pipes. The oscillations in bubble radius and vent pipe pressure are much less pronounced in the 16 mm dia. tube. The observed half period of oscillation for the 16 mm dia. tube is about 50 ms while that for 46 mm dia. tube is about 20 ms. The predicted vent pressure and bubble radius compare within ±15 per cent of the data plotted in figures 6 and 7.

A comparison of the maximum upward pressure observed at the bottom of the test chamber with that predicted by [22] is made in table 1. The maximum upward pressures in table 1 represent the difference between the static pressure and the minimum downward pressure observed at the bottom of the test chamber. It is noted that the predicted upward pressures (uplift) for 95 and 46 mm tubes are 38 and 20 per cent less than the observed pressures. The predicted times of occurrence of maximum uplift are 4 and 6 ms shorter than the observed

Table 1. Comparison of magnitude and time of predicted and observed upward pressure during bubble growth

Vent Pipe Diameter (mm)	Magnitude of Maximum Upward Pressure* kPa		Time of Occurrence (after vent clearing) milliseconds	
	Predicted	Observed	Predicted	Observed
46	2.2	3.5	18	22
95	2.5	3.0	16	22

*Represents difference between static pressure and the minimum pressure observed at the bottom of the test chamber.

times for 46 and 95 mm dia. tubes, respectively. Keeping in mind the uncertainty in the measurements and the approximate nature of the calculation, the predictions are in fair agreement with the data. It may be mentioned that the complete pressure history at the bottom of the test chamber could not be predicted by use of [22] because of the complex fluid motion in the test chamber and the structural oscillations triggered by initial vent clearing process that have not been modeled in this work. Sargis *et al.* (1978) have shown that measure pressures can be affected by the nature of fluid-structure interaction.

4.2 *Effect of placing an additional orifice in the vent line*

When an orifice is placed between the vent exit and the solenoid valve, the vent pipe is divided into two compartments and three additional equations similar to [11], [12] and [13] need to be solved. Figure 8 shows the predicted and observed vent line pressures and bubble growth histories when a 15.6 mm i.d. orifice is placed in the vent line 140 cm away from the vent exit. The reservoir pressure in this case is 177.2 kPa. In figure 8, the zero time corresponds to the time of vent clearing as opposed to the time at which solenoid valve was signaled to open (figures 6 and 7). It is found that predicted static pressures both upstream and downstream of the orifice compare within ±5 per cent of the experimental data. The pressure in the volume between solenoid valve and the orifice is slightly less than reservoir pressure and stays nearly constant with time. The static pressure downstream of orifice is oscillatory and predicted oscillation periods also match fairly well with the data. The predicted bubble radius lies within ±35 per cent of the observed values. Unfortunately, the bubble radius data for the orificed vent line was reduced at larger time intervals and as such predicted oscillations in the bubble radius are not very evident in the data. Coarse nature of the data also fictitiously gives higher difference between the predicted and observed bubble radius.

The predicted vent line static pressure and bubble growth histories with or without an orifice in the vent line are plotted in figure 9. It is observed that placing a 25.4 mm i.d. orifice at 140 cm from the exit, tends to increase the frequency of oscillations in the vent line static pressure and in the bubble radius. However, the magnitude of these oscillations decreases with the insertion

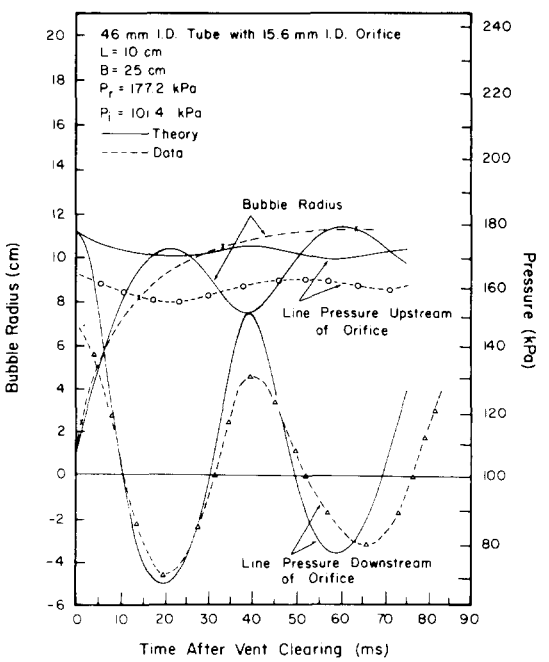

Figure 8. Comparison of theory with observed bubble radius and static line pressures with a 1.56 cm i.d. orifice placed at 140 cm from vent exit.

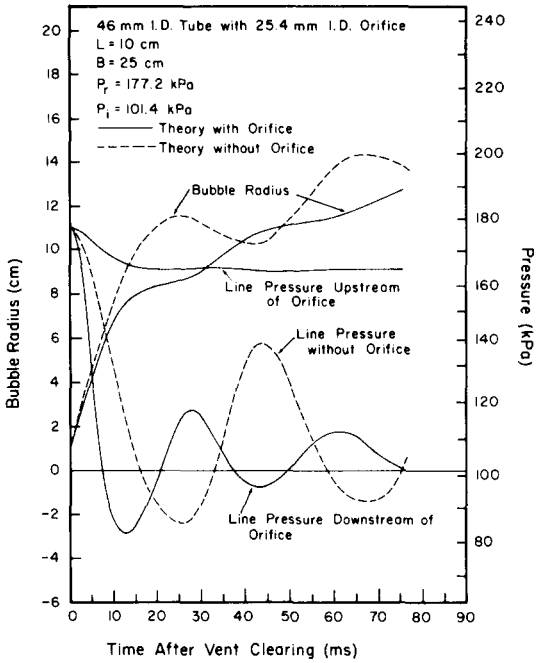

Figure 9. Comparison of theory with observed bubble radius with a 2.54 cm i.d. orifice placed in a 46 mm i.d. tube at 140 cm from vent exit.

of the orifice. The effect of the size of the orifice on the vent pressure and bubble growth characteristic can be inferred from the predictions plotted in figures 8 and 9. It is observed from these figures that reduced size of the orifice increases the magnitude of the pressure oscillations in the pipe volume between the vent exit and the orifice. The increased resistance to flow of the smaller orifice results in larger reduction in the vent pressure during first overexpansion of the bubble. The magnitude of the recovery pressure in the vent pipe after the initial expansion is affected by the bubble inertia. The bubble with smaller orifice shows significant reduction in radius after first overexpansion. This allows for a longer refill period which in turn leads to higher maximum vent pressure. The oscillation period with smaller orifice tends to increase because of longer vent emptying and refill periods. A comparison of the predicted bubble volumes 65 ms after vent clearing shows that bubbles obtained with 25.4 and 15.6 mm dia. orifices will have volumes that are 56 to 49 per cent of the volume of the bubble obtained without presence of an orifice. The flow areas of the orifices on the other hand are 30 per cent and 11 per cent of the flow area of the vent pipe. Thus, the volume of air drawn into a bubble up to 65 ms after vent clearing will not be proportional to area of the orifice. This suggests that apart from affecting the bubble growth and pressure histories, the orifices do not preserve the scaling for volume or mass flux into the bubble which is the sole purpose of placing an orifice in the vent line.

Effect of location of orifice in the vent line is studied in figure 10. The predictions of bubble radius and of static pressure in the vent pipe between the exit and the orifice are for the case when 15.6 mm i.d. orifice is placed at 18.5 cm from the exit of the vent pipe. As compared to the unorificed vent, the vent pressure and bubble growth are more oscillatory in nature. A comparison of the predictions plotted in figure 10 with those in figure 8 shows that moving the orifice closer to the vent exit increases the frequency of oscillations in bubble radius and pressure. However, magnitude of these oscillations is reduced. Bringing the orifice closer to the vent exit inhibits the bubble growth considerably. This is characteristic of the fact that the vent volume between the vent exit and the orifice acts as a capacitor, the emptying or filling rate of which controls the vent pressure and bubble growth histories. While the size of the orifice

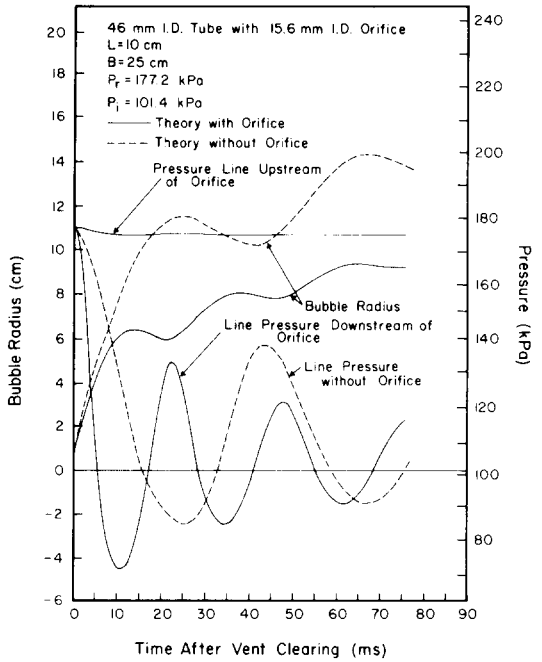

Figure 10. Comparison of bubble radius and static pressures without orifice with a 2.54 cm i.d. orifice placed in a 46 mm i.d. tube at 18.51 cm from vent exit.

introduces a resistance in the flow path, the location of the orifice defines a capacitance in the flow path. The placing of an orifice in the vent pipe can, thus, lead to manifestation of other effects which may not be part of the scaling models.

CONCLUSIONS

(1) Surface of the bubbles formed at the exit of a vent pipe has been observed to oscillate for most of the reservoir pressures studied in this work. The analysis shows that the oscillations occur due to the fact that air flow rate in the vent volume between the solenoid valve and the vent pipe exit cannot keep up with the flow rate needed to sustain inertia associated with the expanding bubble.

(2) The frequency and amplitude of oscillations has been observed to be much less for 16 mm dia. tube than for 46 mm dia. tube.

(3) Predicted time dependent bubble radius and vent pipe static pressure compare within ±35 per cent of all the data. The calculated maximum upward pressures for 46 and 95 mm dia. tubes are 20 per cent and 38 per cent less than the observed pressures. The predicted times of occurrence of the maximum upwards pressure are within 6 ms of the observed times.

(4) Insertion of an orifice in the pipe line between the solenoid valve and the vent exit inhibits the bubble expansion. However, the analysis shows that the reduction in bubble volume is not proportional to the size of the orifice. Presence of an orifice can also affect the oscillatory behavior of the bubble which may not be part of the scaling models.

REFERENCES

ANDERSON, W. G., HUBER, P. W. & SONIN, A. A. 1977 Small scale modeling of hydraulic forces in pressure suppression systems: tests of the scaling laws, 3-594-3-613. Proceedings of Topical Meeting on Thermal Reactor Safety, Sun Valley, Idaho.

BIRKHOFF, G., MARGULIES, R. S. & HORNING, W. A. 1958 Spherical bubble growth. *Phys. Fluids* **1**, 201–206.

CHAN, C. K., DHIR, V. K., LIU, C. Y. & CATTON, I. 1977 Suppression pool dynamics, NUREG-0264-3.

CHEN, C. L. 1979 Hydrodynamics of a bubble growing at vent pipe exit. M.S. Thesis, University of California, Los Angeles.

DAVIDSON, J. F. & SCHULER, O. G. 1960 Bubble formation at an orifice in a viscous liquid. *Trans. Inst. Chem. Engrs* **38**, 144–154.

DAVIDSON, J. F. & SCHULER, O. G. 1960 Bubble formation at an orifice in an inviscid liquid. *Trans. Inst. Chem. Engrs* **38**, 335–352.

DHIR, V. K., CHAN, C. K. & CATTON, I. 1977 Air bubble behavior and associated hydrodynamic forces during vent clearing in a BWR suppression pool, 3-665-3-682. Proceedings of Topical Meeting on Thermal Reactor Safety, Sun Valley, Idaho.

FORSTER, H. K. & ZUBER, N. 1954 Growth of a vapor bubble in a superheated liquid. *J. Appl. Phys.* **25**, 474–478.

GILMORE, F. R. 1952 The growth or collapse of a spherical bubble in a viscous compressible liquid. Rep. 26-4 Hydrodynamics Lab., California Institute of Technology, Pasadena, California, U.S.A.

HERRING, C. 1941 Theory of the pulsation of gas bubble produced by an underwater explosion. NDRC Division 6 Report CA-Sr20.

KIANG, R. L. & GROSSI, B. J. 1978 Three dimensional pool swell modeling of a Mark I suppression pool system. EPRI NP-906.

LAMB, H. 1945 *Hydrodynamics*, 6th Edn. Dover, New York.

MCCANN, D. J. & PRINCE, R. G. H. 1969 Bubble formation and weeping at a submerged orifice. *Chem. Eng. Science* **24**, 801–814.

PLESSET, M. S. & ZWICK, S. A. 1954 The growth of vapor bubbles in superheated liquids. *J. Appl. Phys.* **25**, 493–500.

RAMAKRISHNAN, S., KUMAR, R. & KULOOR, N. R. 1969 Studies in bubble formation under constant flow conditions. *Chem. Engng Sci.* **24**, 731–747.

RAYLEIGH, LORD M. 1917 On the pressure developed in a liquid during the collapse of a spherical cavity. *Phil. Mag.* **34**, 94–98.

SARGIS, D. A., STUHMULLER, J. H. & WANG, S. S. 1978 A fundamental thermal-hydraulic model to predict steam chugging phenomena. Topics in two phase heat transfer and flow, *ASME Winter Annual Meeting*, pp. 123–133. San Francisco.

SATYANARAYAN, A., KUMAR, R. & KULOOR, N. R. 1969 Studies in bubble formation—II. Bubble formation under constant pressure conditions. *Chem. Engng Sci.* **24**, 749–761.

SCRIVEN, L. E. 1959 On the dynamics of bubble growth. *Chem. Engng Sci.* **10**, 1–13.

SHAPIRO, A. M. 1953 *Dynamics and Thermodynamics of Compressible Fluid Flow*. The Ronald Press, New York.

WEISSHANPL, 1972 Formation and oscillation of a gas bubble under water. Aeg-Telefunken Report No. 2241.